Electronic Supplementary Material (ESI) for Physical Chemistry Chemical Physics.

Supplementary Material: Probing the location of the unpaired electron in spin-orbit changing collisions of NO with Ar

Cornelia G. Heid,[1] Imogen P. Bentham,[1] Victoria Walpole,[1, a)] Razvan Gheorghe,[1] Pablo G. Jambrina,[2] F. Javier Aoiz,[3] and Mark Brouard[1, b)]

[1)]*Department of Chemistry, University of Oxford, The Chemistry Research Laboratory, 12 Mansfield Road, Oxford, OX1 3TA, United Kingdom*

[2)]*Departamento de Química Física, Universidad de Salamanca, 37008, Salamanca, Spain*

[3)]*Departamento de Química Física, Facultad de Química, Universidad Complutense, 28040 Madrid, Spain*

[a)]Current address: Max Planck Institute for Biophysical Chemistry, Am Faßberg 11, 37077 Göttingen, Germany

[b)]Electronic mail: mark.brouard@chem.ox.ac.uk.

A. Theory

In the helicity representation, the scattering amplitude for a transition from an initial state $|jm|\Omega|\varepsilon\rangle$ to a final state $|j'm'|\Omega'|\varepsilon'\rangle$ can be written as:

$$f_{j'm'\Omega'\varepsilon',jm\Omega\varepsilon}(\theta) \equiv F_{m'\varepsilon'm\varepsilon} = \frac{1}{2ik_{\text{in}}} \sum_J (2J+1) d^J_{m'm}(\theta)\, S^J_{j'm'\Omega'\varepsilon',jm\Omega\varepsilon} \ , \tag{1}$$

where θ is the scattering angle (the angle between the initial and final relative velocities, $\boldsymbol{k}$ and $\boldsymbol{k}'$) and j, m, $|\Omega|$, and ε are the quantum numbers that represent, respectively, the total rotational angular momentum quantum number apart from nuclear spin, its projection onto $\boldsymbol{k}$, the absolute value of the spin-orbit quantum number, and the symmetry index (e/f). The primes indicate the respective product labels. k_{in} is the initial relative wave vector, $d^J_{m'm}(\theta)$ is the element of the reduced rotation matrix, and $S^J_{j'm'\Omega'\varepsilon',jm\Omega\varepsilon}$ is the scattering matrix element for the indicated transition.

We can define a J dependent scattering amplitude,

$$F^J_{m'\varepsilon' m\varepsilon} = \frac{1}{2ik_{\text{in}}} (2J+1) d^J_{m'm}(\theta) S^J_{j'm'\Omega'\varepsilon',jm\Omega\varepsilon} \ , \tag{2}$$

and express the scattering amplitude $F_{m'\varepsilon'm\varepsilon}$ (for fixed values of j, j', $|\Omega|$, and $|\Omega'|$) as

$$F_{m'\varepsilon' m\varepsilon} = \sum_J F^J_{m'\varepsilon' m\varepsilon} \ . \tag{3}$$

We can also define the sum of the scattering amplitude products over m' as

$$Q_{m_1\varepsilon_1 m_2\varepsilon_2} \equiv \sum_{m'} F_{m'\varepsilon'm_1\varepsilon_1} F^*_{m'\varepsilon'm_2\varepsilon_2} = \sum_{J_1}\sum_{J_2} Q^{J_1J_2}_{m_1\varepsilon_1 m_2\varepsilon_2} \ , \tag{4}$$

where

$$Q^{J_1J_2}_{m_1\varepsilon_1 m_2\varepsilon_2} = \sum_{m'} F^{J_1}_{m'\varepsilon'm_1\varepsilon_1} \left[F^{J_2}_{m'\varepsilon'm_2\varepsilon_2}\right]^* \ . \tag{5}$$

Summing over m' and averaging over initial m, we obtain the differential cross section (DCS) for a $j\Omega\varepsilon \rightarrow j'\Omega'\varepsilon'$ transition:

$$\mathrm{d}\sigma(j\Omega\varepsilon \rightarrow j'\Omega'\varepsilon') = \frac{1}{(2j+1)} \sum_m \sum_{m'} |F_{m'\varepsilon'm\varepsilon}|^2 = \frac{1}{(2j+1)} \sum_m Q_{m\varepsilon m\varepsilon} \tag{6}$$

For $j = \frac{1}{2}$,

$$\mathrm{d}\sigma(\frac{1}{2}\Omega\varepsilon \rightarrow j'\Omega'\varepsilon') = \frac{1}{2}\sum_{m=-1/2}^{1/2} Q_{m\varepsilon\, m\varepsilon} = Q_{1/2\varepsilon\, 1/2\varepsilon}\ , \tag{7}$$

since $Q_{m\varepsilon_1\, m\varepsilon_2} = \varepsilon_1\varepsilon_2 Q_{-m\varepsilon_1\, -m\varepsilon_2}$.

As introduced in the main text, in the presence of an orienting electric field, a pure f Λ-doublet state becomes a superposition of the two Λ-doublet states:

$$|jm_E|\Omega|E\rangle = \frac{1}{\sqrt{2}}\left[\alpha(E)\,|jm_E|\Omega|e\rangle + \beta(E)\,|jm_E|\Omega|f\rangle\right]\ , \tag{8}$$

where m_E is the projection of $\boldsymbol{j}$ onto the electric field vector $\boldsymbol{E}$, and the coefficients $\alpha(E)$ and $\beta(E)$ are the field-dependent mixing parameters, such that $\alpha^2 + \beta^2 = 2$. In the infinite field limit, that is, when $W_{\mathrm{Stark}} \gg E_\Lambda$ (where W_{Stark} is the linear Stark effect for a pure f Λ-doublet and E_Λ is the Λ-doublet splitting), $|\alpha| = |\beta| = 1$.

The rotational state with its projection along $\boldsymbol{E}$ can be written in terms of those states whose quantization axis is taken along $\boldsymbol{k}$:

$$|jm_E\Omega\varepsilon\rangle = \sum_m D^j_{m m_E}(\phi_E, \theta_E, 0)|jm\Omega\varepsilon\rangle\,, \tag{9}$$

where $D^j_{m m_E}(\phi_E, \theta_E, 0)$ is the rotation matrix element, with the angles θ_E and ϕ_E relating the LAB frame $(Z||\boldsymbol{E})$ to the scattering frame $(z||\boldsymbol{k})$. Accordingly, the polar, θ_E, and azimuthal, ϕ_E, angles define the direction of the electric field in the $\boldsymbol{k}$-$\boldsymbol{k}'$ scattering frame.

As demonstrated in ref. 1 and 2, the orientation dependent DCS for $j = \frac{1}{2}$ in the presence of a static electric field can be written as:

$$\left[\mathrm{d}\sigma(\frac{1}{2}|m_E|\Omega\hat{E} \rightarrow j'\Omega'\varepsilon')\right]_{\theta_E}^{\phi_E} = \frac{1}{2}\Big\{\alpha^2 Q_{1/2\,e\,1/2e} - |\alpha\beta|\Big[\cos\theta_E\left(Q_{1/2f\,1/2e} + Q_{1/2e\,1/2f}\right) + \sin\theta_E\cos\phi_E(Q_{-1/2f\,1/2e} + Q_{1/2e\,-1/2f})\Big] + \beta^2 Q_{1/2\,f\,1/2f}\Big\}\ , \tag{10}$$

and the r-polarization dependent differential cross sections (r-PDDCSs), $R_q^{(k)}(\theta)$,[3] can be written in terms of the $Q_{m_1\,\varepsilon_1\,m_2,\varepsilon_2}$ products,

$$\frac{\sigma_{\mathrm{iso}}}{2\pi}R_0^{(0)}(\theta) = \frac{1}{2}(\alpha^2 Q_{1/2e\,1/2e} + \beta^2 Q_{1/2f\,1/2f}) \tag{11}$$

$$\frac{\sigma_{\mathrm{iso}}}{2\pi}R_0^{(1)}(\theta) = \frac{1}{2}(Q_{1/2f\,1/2e} + Q_{1/2e\,1/2f}) \tag{12}$$

$$\frac{\sigma_{\mathrm{iso}}}{2\pi}R_1^{(1)}(\theta) = -\frac{1}{2\sqrt{2}}(Q_{-1/2f\,1/2e} + Q_{1/2e\,-1/2f})\ , \tag{13}$$

where $\sigma_{\rm iso}$ is the isotropic integral cross section (ICS) in the presence of the orienting field. Substituting eqn (11)-(13) into eqn (10), the orientation dependent DCS can then be written in terms of the r-PDDCSs:[1,2]

$$[\mathrm{d}\sigma(\theta)]_{\theta_E}^{\phi_E} = \frac{\sigma_{\rm iso}}{2\pi}\left[R_0^{(0)}(\theta) - |\alpha\beta|\Big(\cos\theta_E R_0^{(1)}(\theta) - \sqrt{2}\sin\theta_E\cos\phi_E R_1^{(1)}(\theta)\Big)\right], \tag{14}$$

where we have used $[\mathrm{d}\sigma(\theta)]_{\theta_E}^{\phi_E} \equiv \left[\mathrm{d}\sigma(\frac{1}{2}|m_E|\Omega\hat{E} \rightarrow j'\Omega'\varepsilon')\right]_{\theta_E}^{\phi_E}$ to simplify the notation.

As discussed in the main text, the $R_0^{(1)}(\theta)$ and $R_1^{(1)}(\theta)$ moments quantify orientation along the z- and x-axes, respectively, while $R_0^{(0)}(\theta)$ represents the isotropic moment. When $\theta_E = 90^\circ$ and $\phi_E = 90^\circ$, that is, when $\boldsymbol{E}$ is along the $\pm y$ axis, perpendicular to the $\boldsymbol{k}$-$\boldsymbol{k}'$ plane, $R_0^{(0)}(\theta)$ is the only surviving moment. It should be noted that, as long as $|\alpha\beta| \neq 0$, $(\sigma_{\rm iso}/2\pi)R_0^{(0)}(\theta)$ does not coincide with the DCS obtained in the absence of an orienting field. Only when $\alpha = 0$, and hence $\beta = 2$, or $\alpha = 2$ and $\beta = 0$, the respective DCSs are those of the initial $\varepsilon = f$ and $\varepsilon = e$ pure states.

Making use of eqn (4), eqn (10) can be rewritten as

$$\begin{aligned}\Big[\mathrm{d}\sigma(\theta)\Big]_{\theta_E}^{\phi_E} = \frac{1}{2}\sum_{J_1,J_2}\Big\{&\alpha^2 Q^{J_1J_2}_{1/2e\,1/2e} - |\alpha\beta|\Big[\cos\theta_E(Q^{J_1J_2}_{1/2f\,1/2e} + Q^{J_1J_2}_{1/2e\,1/2f}) + \\ &\sin\theta_E\cos\phi_E(Q^{J_1J_2}_{-1/2f\,1/2e} + Q^{J_1J_2}_{1/2e\,-1/2f})\Big] + \beta^2 Q^{J_1J_2}_{1/2f\,1/2f}\Big\},\end{aligned} \tag{15}$$

which for convenience can be recast as,[4]

$$\begin{aligned}\Big[\mathrm{d}\sigma(\theta)\Big]_{\theta_E}^{\phi_E} = \frac{1}{2}\sum_{J}\sum_{J_1,J_2}\frac{\delta_{J,J_1}+\delta_{J,J_2}}{2}\Big\{&\alpha^2 Q^{J_1J_2}_{1/2e\,1/2e} + \beta^2 Q^{J_1J_2}_{1/2f\,1/2f} - \\ &|\alpha\beta|\Big[\cos\theta_E(Q^{J_1J_2}_{1/2f\,1/2e} + Q^{J_1J_2}_{1/2e\,1/2f}) + \\ &\sin\theta_E\cos\phi_E(Q^{J_1J_2}_{-1/2f\,1/2e} + Q^{J_1J_2}_{1/2e\,-1/2f})\Big]\Big\}.\end{aligned} \tag{16}$$

In a previous work,[4,5] it was shown that it is possible to define a quantum generalized deflection function (QM GDF), a quantum analog to the classical joint probability distribution of the scattering angle and the total angular momentum. For a specific $|j = \frac{1}{2}, |\Omega| = \frac{1}{2}, \varepsilon\rangle \rightarrow |j'|\Omega'|\varepsilon'\rangle$ transition, the QM GDF, $Q(\theta, J; \varepsilon)$, can be written as:

$$Q(\theta, J; \varepsilon) = \frac{\sin\theta}{2j+1}\sum_{J_1}\sum_{J_2}\sum_{m}\frac{\delta_{J_1,J}+\delta_{J_2,J}}{2} \times Q^{J_1J_2}_{m\varepsilon,m\varepsilon}, \tag{17}$$

where the final state quantum numbers have been omitted for simplicity.

The QM GDF can be considered as a joint quasi-probability distribution that allows quantum dynamicists to investigate the simultaneous dependence of a scattering process on the total angular momentum J and the scattering angle θ. Quantum mechanical results can thus be used to shed light on the reaction or scattering mechanism. In many cases, there is good agreement between the quantum and classical correlation functions, as long as quantum effects are not dominant. As shown in detail in refs. 4 and 5, it is possible to calculate a polarization dependent quantum deflection function. For $j = \frac{1}{2}$, the orientation dependent QM GDF can be written as:

$$\left[Q(\theta,J)\right]_{\theta_E}^{\phi_E} = \frac{\sin\theta}{2}\sum_{J_1}\sum_{J_2}\frac{\delta_{J_1,J}+\delta_{J_2,J}}{2}\Big\{\alpha^2 Q^{J_1J_2}_{1/2e\,1/2e} + \beta^2 Q^{J_1J_2}_{1/2f\,1/2f} - |\alpha\beta|\Big[\cos\theta_E\,(Q^{J_1J_2}_{1/2f\,1/2e} + Q^{J_1J_2}_{1/2e\,1/2f}) + \sin\theta_E\cos\phi_E\,(Q^{J_1J_2}_{-1/2f\,1/2e} + Q^{J_1J_2}_{1/2e\,-1/2f})\Big]\Big\}\,. \tag{18}$$

The resulting interference pattern may be very sensitive to small changes in the polarized distribution of the reactants, and the interference effects on the corresponding differential cross sections are generally more pronounced than for an isotropic distribution of reactants. As discussed in ref. 4, the QM GDF, $\left[Q(\theta,J)\right]_{\theta_E}^{\phi_E}$, are additive over J, although they can take on negative values.

Finally, by integrating eqn (18) over θ, we can extract the J-partial cross section,

$$\left[\widetilde{\sigma}(J)\right]_{\theta_E}^{\phi_E} = \int_0^{\pi}\left[Q(\theta,J)\right]_{\theta_E}^{\phi_E}\mathrm{d}\theta = \frac{1}{2\,k_{\mathrm{in}}^2}(2J+1)\left[\widetilde{P}(J)\right]_{\theta_E}^{\phi_E}\,. \tag{19}$$

It must be stressed that, in general, the orientation dependent partial cross section, $\left[\widetilde{\sigma}(J)\right]_{\theta_E}^{\phi_E}$ (or the collision probability, $\left[\widetilde{P}(J)\right]_{\theta_E}^{\phi_E}$), does not have azimuthal symmetry and integration is only carried out over θ. Only in those cases in which $m_1 = m_2$, that is, if only $R_q^{(k)}(\theta)$ moments with $q = 0$ intervene, is the azimuthal symmetry preserved and $\left[\widetilde{\sigma}(J)\right]_{\theta_E}^{\phi_E}$ is a truly orientation dependent partial cross section. The expressions for the r-polarization dependent QM GDFs are entirely analogous to those of the r-PDDCSs. In particular, for $j = \frac{1}{2}$, the respective expressions

are equivalent to those in eqn (11)-(13):

$$\frac{\sigma_{\rm iso}}{2\pi}Q_0^{(0)}(\theta,J) = \frac{1}{2}\sum_{J_1}\sum_{J_2}\frac{\delta_{J_1,J}+\delta_{J_2,J}}{2}(\alpha^2 Q^{J_1J_2}_{1/2e\,1/2e} + \beta^2 Q^{J_1J_2}_{1/2f\,1/2f}) \tag{20}$$

$$\frac{\sigma_{\rm iso}}{2\pi}Q_0^{(1)}(\theta,J) = \frac{1}{2}\sum_{J_1}\sum_{J_2}\frac{\delta_{J_1,J}+\delta_{J_2,J}}{2}(Q^{J_1J_2}_{1/2f\,1/2e} + Q^{J_1J_2}_{1/2e\,1/2f}) \tag{21}$$

$$\frac{\sigma_{\rm iso}}{2\pi}Q_1^{(1)}(\theta,J) = -\frac{1}{2\sqrt{2}}\sum_{J_1}\sum_{J_2}\frac{\delta_{J_1,J}+\delta_{J_2,J}}{2}(Q^{J_1J_2}_{-1/2f\,1/2e} + Q^{J_1J_2}_{1/2e\,-1/2f})\,. \tag{22}$$

B. Integral steric asymmetries (ISA) for $\Delta\Omega = 0$ and $\Delta\Omega = 1$

Supplementary Fig. S1 compares the QM integral steric asymmetries for the spin-orbit conserving (dark cyan) and spin-orbit changing (red) manifold in the side-on (top) and the end-on (bottom) configurations. The data were calculated at the experimental field strength, and the spin-orbit changing ISAs are the same as the ones shown in Fig. 3 of the main text. A positive value corresponds to a preference for N-side ($+x$) and N-end ($-z$) collisions in the side-on and end-on orientations, respectively. While the oscillations of the ISAs in the spin-orbit conserving manifold are roughly centered around zero, the ISAs for the spin-orbit changing manifold are shifted towards positive values.

A different view of the overall preference for N-side/N-end collisions is given in Fig. S2. In this figure, the DCSs for the two side-on and the two end-on orientations have been summed over all even (top) and all odd (bottom) energetically accessible states in the spin-orbit changing manifold. For the odd Δj transitions, the summed DCSs for the $+x$ (red) ad the $-z$ (green) orientations are clearly larger than the ones for the opposite orientations. Although, in the side-on orientation, the $-x$ (blue) configuration becomes more important at larger scattering angles, the $+x$ orientation is dominant up to $\theta \sim 70^\circ$. The differences between the summed DCSs for even Δj transitions are less stark; however, it is again the $+x$ and the $-z$ orientations that dominate. This confirms our conclusion that collisions towards the N-side/N-end of the NO molecule are overall preferred owing to the increased electron density closer to the N-end.

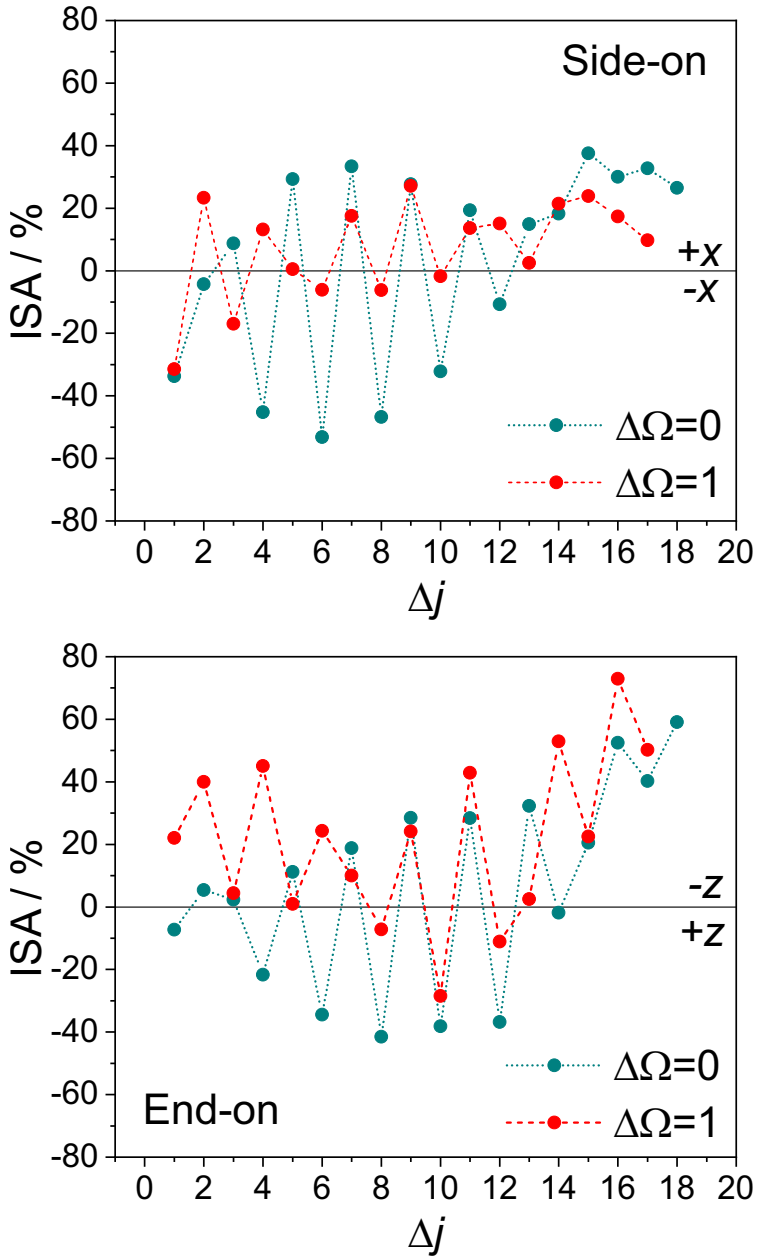

Fig. S 1. Comparison of the QM integral steric asymmetries for the spin-orbit conserving ($\Delta\Omega = 0$, dark cyan) and changing ($\Delta\Omega = 1$, red) manifolds in the side-on (top) and the end-on (bottom) geometries. Both sets of data are for the e final states at the experimental field strength and have been averaged over the experimental collision energy distribution.

C. J-partial cross sections and opacity functions

The J-partial cross sections, calculated according to eqn (19), are presented in Fig. S3 for the same states and orientations as in Fig. 4 of the main text. These partial cross sections represent the contribution of each J to the differential cross section of a specific final rotational state. The

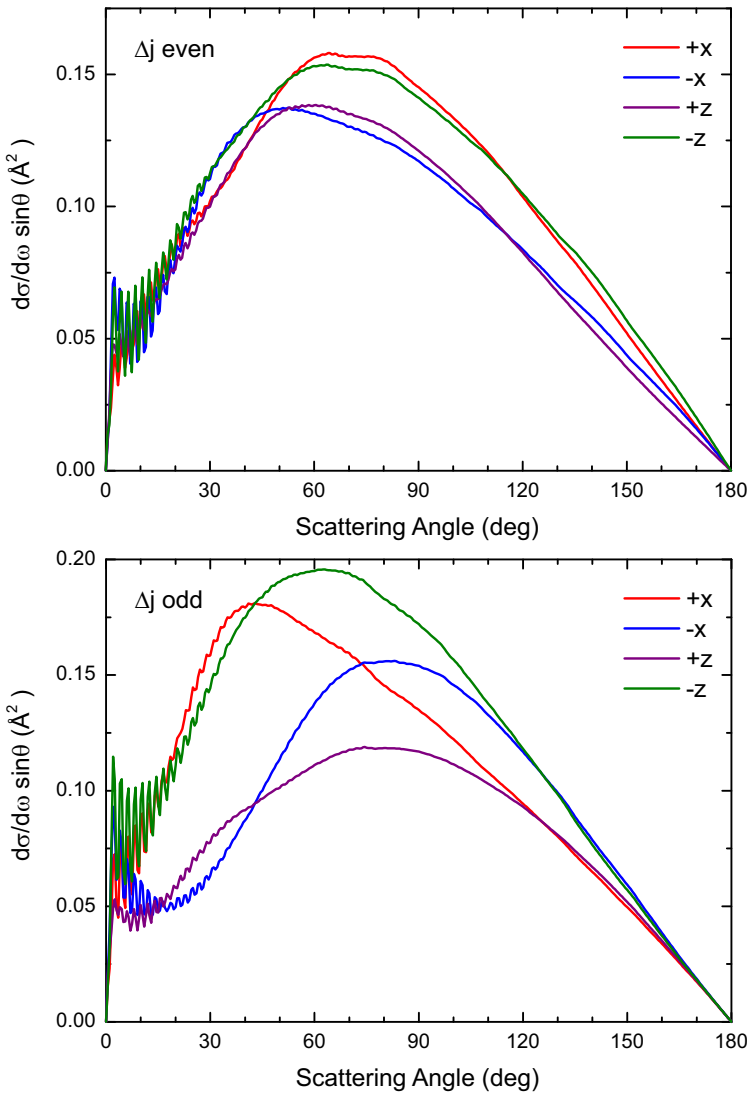

Fig. S2. Sums of the infinite field DCSs for even (top) and odd (bottom) Δj transitions into the spin-orbit changing manifold. The DCSs have been summed over the energetically accessible even/odd Δj states. The $+x$, $-x$, $+z$, and $-z$-orientations are represented in red, blue, purple, and green, respectively.

isotropic distribution in the presence of the electric field is included in black. For initial $j = \frac{1}{2}$, J is approximately equal to the orbital angular momentum, and hence proportional to the classical impact parameter.

The odd Δj transitions, shown in the bottom two rows of Fig. S3, exhibit a clear preference for $+x$ (red) and $-z$ (green), respectively. In contrast, the J-partial cross sections for even Δj transitions, plotted in the top two rows, are more similar for the two side-on and the two end-on orientations. The J-partial cross sections for $\Delta j = 6, 8, 10$ show a maximum in the $+z$ orientation

(purple) at high impact parameters, which, as seen more clearly in Fig. 5 of the main text, is correlated with the strong forward scattered peak.

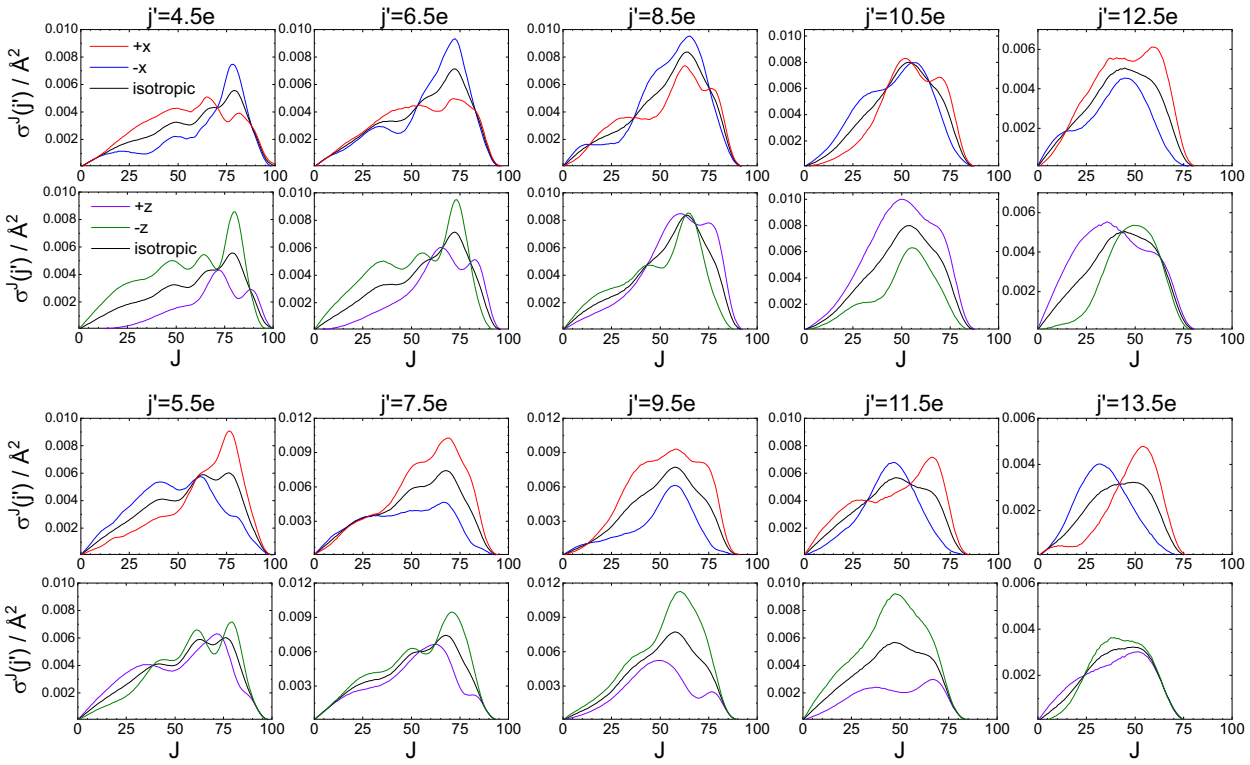

Fig. S 3. Comparison of the $\pm x$ and $\pm z$ J-partial cross sections for $\Delta j = 4 - 13$ ($\Delta\Omega = 1$), calculated at infinite field strength. The partial cross sections, as a function of total angular momentum, J, for the side-on configuration (red: $+x$, blue: $-x$) and for the end-on configuration (purple: $+z$, green: $-z$) are shown in the first/third and second/fourth row, respectively. The isotropic distribution in the field is indicated in black.

The correlation between impact parameter and scattering angle is further examined in Fig. S4 for the $j' = 7.5e$ and $j' = 8.5e$ final states. The trends are similar for the other j' transitions. The DCSs, shown in columns 1 and 3 of the figure, are multiplied by $\sin\theta$ to be compared with the J-partial cross sections (calculated according to eqn (19)), shown in columns 2 and 4. Transitions within the spin-orbit conserving manifold are indicated in red, and transitions within the spin-orbit changing manifold in blue. As can be seen, the DCSs are almost mirror images of the J-partial cross sections, reflecting the strong correlation between J and θ that is also observed in Fig. 5 in the main text.

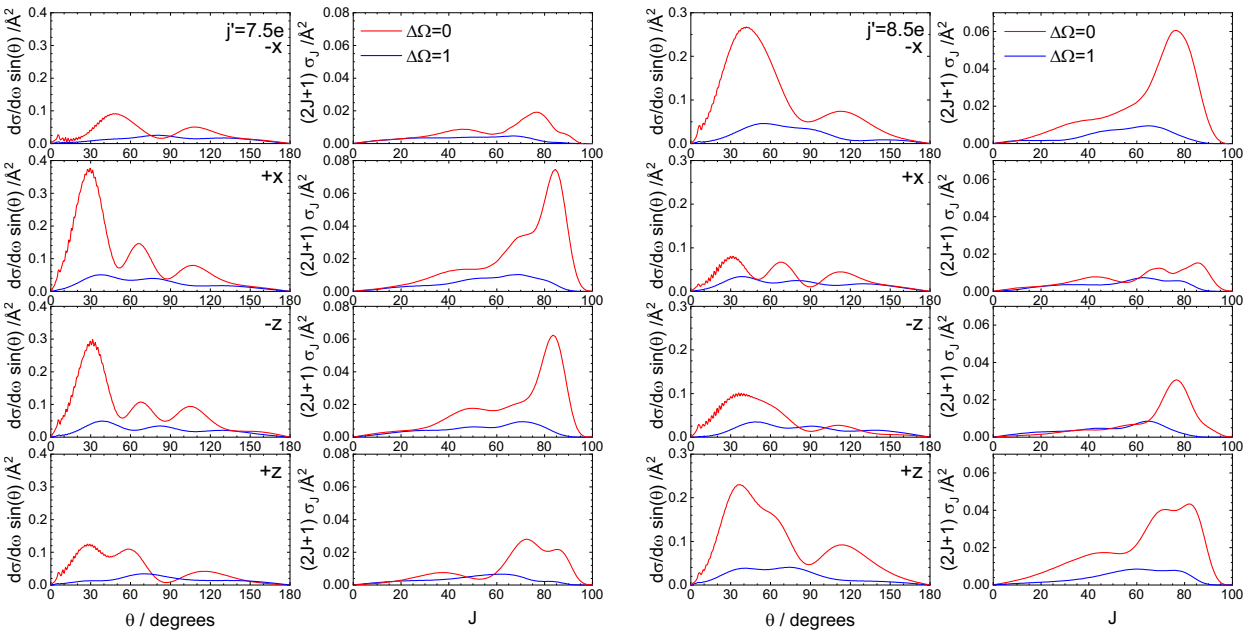

Fig. S 4. Comparison between the calculated DCSs (weighted by $\sin\theta$) and the corresponding J-partial cross sections for $j' = 7.5e$ (left panels) and $j' = 8.5e$ (right panels). The $-x$, $+x$, $-z$, and $+z$ orientations are shown top to bottom, with the spin-orbit conserving transitions ($\Delta\Omega = 0$) represented in red, and the spin-orbit changing transitions ($\Delta\Omega = 1$) in blue.

D. Modified potential calculations

The differential cross sections on the modified potentials have been calculated analogously to the DCSs on the full potentials. To remove the attractive parts of the PES, the A′, A″, and full potentials were multiplied with a scaling factor, defined by a parameterized log sigmoid function of the form[6]

$$f(R, R_0, R_{\text{shift}}, \eta) = 1 - \frac{1}{1 + \exp(-\eta(R - R_0 + R_{\text{shift}}))} \,. \tag{23}$$

Here, R is the distance between the center of mass of the NO molecule and the Ar atom, R_0 corresponds to the PES contour at zero collision energy, and R_{shift} shifts the inflection point to smaller R. The value of η determines the steepness of the function and was chosen such that the contour at the collision energy in the modified potential remained the same as in the unmodified potential. The specific values used to scale the potentials were $\eta = 10\,\text{bohr}^{-1}$ and $R_{\text{shift}} = 0.4$ bohr. The DCSs calculated on the modified PESs are shown in Fig. S5 for the O-end orientation (in which the forward feature is observed most prominently on the full PES). The prominent forward

peak is completely absent in those DCSs, providing strong evidence that the attractive parts of the potential are essential for the occurrence of the peak.

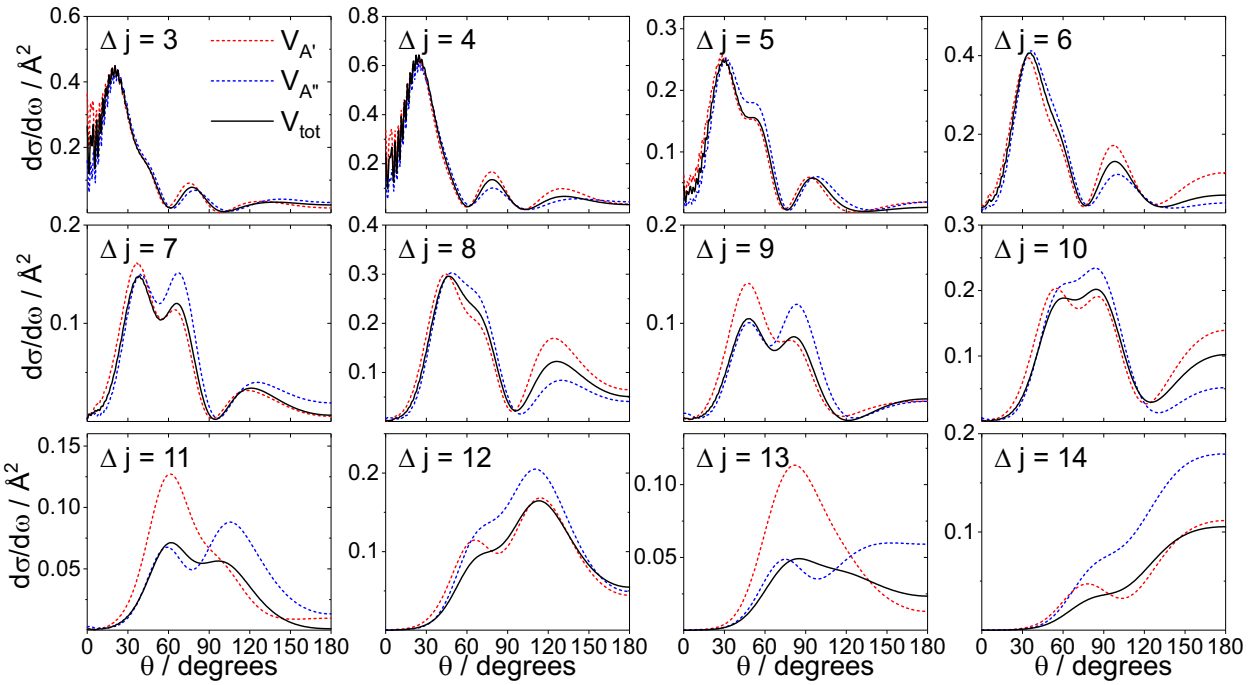

Fig. S 5. QM DCSs for the O-end orientation calculated on the modified PESs, with the attractive parts removed, for $\Delta j = 3 - 14$ (final e states). The black trace represents the DCS calculated on the truncated total potential (including V_{sum} and V_{dif}); the red and blue dashed traces represent the DCSs obtained on the truncated A′ and A″ potentials, respectively. All data are for the spin-orbit conserving transitions. Note that the prominent forward scattered peak observed in the DCSs on the full potential is missing, indicating that the attractive parts of the PES are crucial for the occurrence of this feature.

E. QM hardshell (QMHS) model calculations

In the quantum mechanical hardshell model,[7,8] atoms and diatomic molecules are approximated as rigid bodies, and any long range attractive forces are entirely neglected. In scattering processes for which the attractive parts of the potential are unimportant, the model has been shown to be a good approximation to the full QM calculation.[7] Due to the removal of the attractive parts, QMHS calculations should be comparable with calculations run on the truncated PESs.

The QMHS DCSs of an unoriented ensemble of NO molecules were calculated using the PES contours at the experimental collision energy of 651 cm^{-1}, treating the NO molecule as a closed-

shell species. (Currently, the formalism only applies to closed-shell molecules; the calculations were therefore run on the V_{sum}, rather than the full PES). Rotational states up to $j' = 21$ and partial waves up to $J = 120$ were included in the close-coupled equations. The results obtained on the A′, A″, and sum potentials are presented in Fig. S6. The DCSs are in qualitative agreement with the ones calculated on the modified potentials in Fig. S5. Any differences may be attributed to the fact that in Fig. S5 the molecules are oriented, while in Fig. S6 the initial distribution of the molecules is isotropic. Once again, the absence of features in the very forward scattered region, particularly in the A′ potential calculations, provides strong evidence that the attractive parts of the potential are instrumental for the appearance of the prominent forward peak observed in the full PES calculations for the spin-orbit changing transitions.

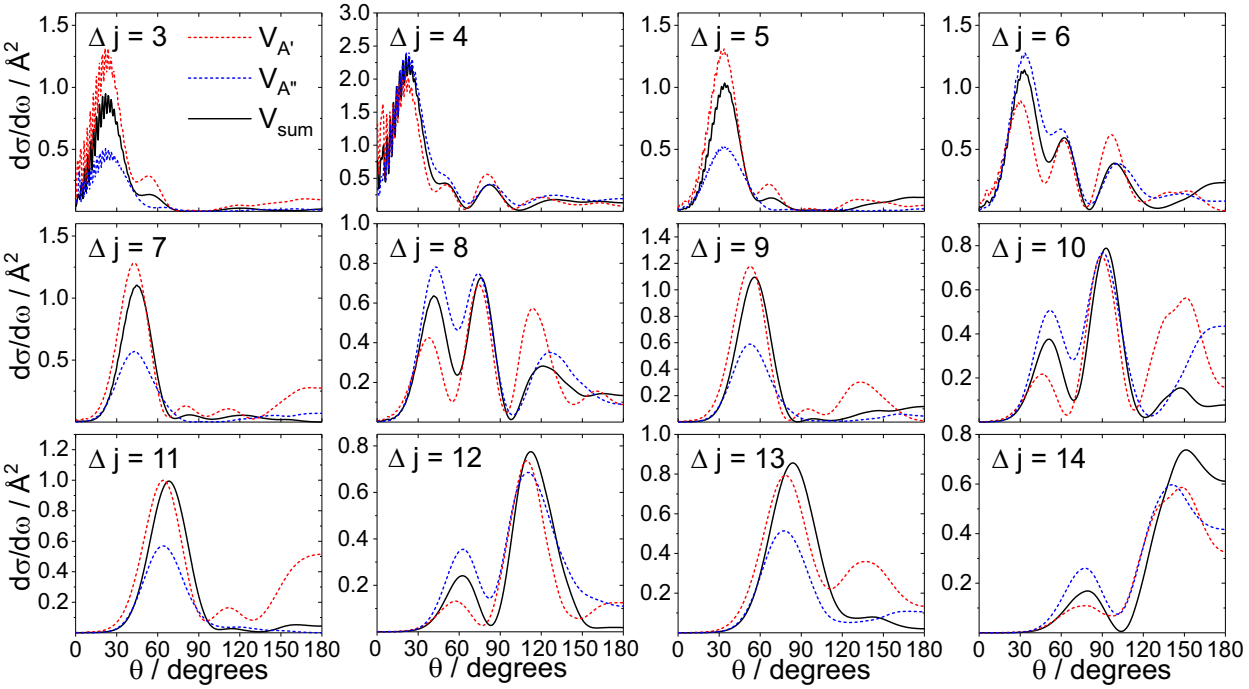

Fig. S6. Isotropic (closed-shell) hardshell QM DCSs calculated on the A′ (red dashed line), A″ (blue dashed line), and sum (black line) potentials for $\Delta j = 3 - 14$. The hardshell was defined as the contour of the full PES at the mean experimental collision energy of 651 cm^{-1}. The DCSs are similar to the ones calculated on the soft potential, with the prominent forward scattered peak missing.

REFERENCES

[1]C. G. Heid, V. Walpole, M. Brouard, F. J. Aoiz and P. G. Jambrina, *Nat. Chem.*, 2019, **11**, 662–668.

[2]V. Walpole, C. G. Heid, P. G. Jambrina, F. J. Aoiz and M. Brouard, *J. Phys. Chem. A*, 2019, **123**, 8787–8806.

[3]F. J. Aoiz, M. T. Martínez and V. Sáez Rábanos, *J. Chem. Phys.*, 2001, **114**, 8880–8896.

[4]P. G. Jambrina, M. Menéndez and F. J. Aoiz, *Chem. Sci.*, 2018, **9**, 4837–4850.

[5]P. G. Jambrina, M. Menéndez, A. Zanchet, E. García and F. J. Aoiz, *Phys. Chem. Chem. Phys.*, 2019, **21**, 14012–14022.

[6]M. Brouard, H. Chadwick, C. J. Eyles, B. Hornung, B. Nichols, J. M. Scott, F. J. Aoiz, J. Kłos, S. Stolte and X. Zhang, *Mol. Phys.*, 2013, **111**, 1759–1771.

[7]S. D. Bosanac and N. Petrović, *Phys. Rev. A*, 1990, **41**, 5909.

[8]M. Brouard, B. Hornung and F. J. Aoiz, *Phys. Rev. Lett.*, 2013, **111**, 183202.